CASE 55

Optimization of a Linear Actuator Using Simulation

Abstract: Since the structure of magnetic circuits is advanced and complicated, it is difficult to design magnetic circuits without finite-element method (FEM) analysis. In our research, by integrating FEM magnetic field analysis and quality engineering, we designed parameters of a magnetic circuit to secure its robustness through the evaluation of reproducibility not only in simulation but also in an actual device. Additionally, we found that reducing cost and development cycle time was possible using this process.

1. Introduction

Figure 1 depicts a circuit of a magnetic drive system. The magnetic circuit used for this research was cylindrical and horizontally symmetric. Therefore, when electric current is not applied, static thrust is balanced in the center position with magnetic force generated by magnets. On the other hand, once electric current is applied, one-directional thrust is produced by the imbalance of force caused by magnetic flux around a coil. The direction of thrust can be controlled by the direction of current. As illustrated in Figure 2, it is ideal that static thrust, y, be proportional to input current, M, as well as a large amount of thrust by a small input of current.

In our research, by using static simulation software for magnetic drive, which was developed inhouse, instead of conducting an actual experiment, we implemented parameter design. After selecting an optimal configuration, we confirmed reproducibility in simulation and in an actual device.

2. Design of Experiments for Simulation

Based on the parameters in Figure 3, we created Figure 4, a *Y*-type cause-and-effect diagram for design of experiment.

Signal Factors and Characteristic

According to the definition of an ideal state, we selected current (M_1, M_2, M_3) as a signal factor and static thrust as a characteristic.

Control Factors

We chose design parameters associated with a magnetic drive structure as control factors and set levels for each factor (Table 1).

Noise Factors

We set dimensional variability of design parameters as a substitute for stresses of an actual device (Figure 4). More specifically, for each design parameter, we set two levels, one a certain variability above a nominal design parameter and the other below a nominal. As a next step, by conducting a preliminary experiment with an L_{12} orthogonal array (Table 2), we studied a magnitude of effects on the characteristic and a trend for each level of each factor (from Table 3). Using the data of the preliminary experiment, we calculated factor effects in Table 4 and plotted them in Figure 5.

Indicative Factors

Essentially, stroke affects the conversion efficiency rate of static thrust for electric current and it is de-

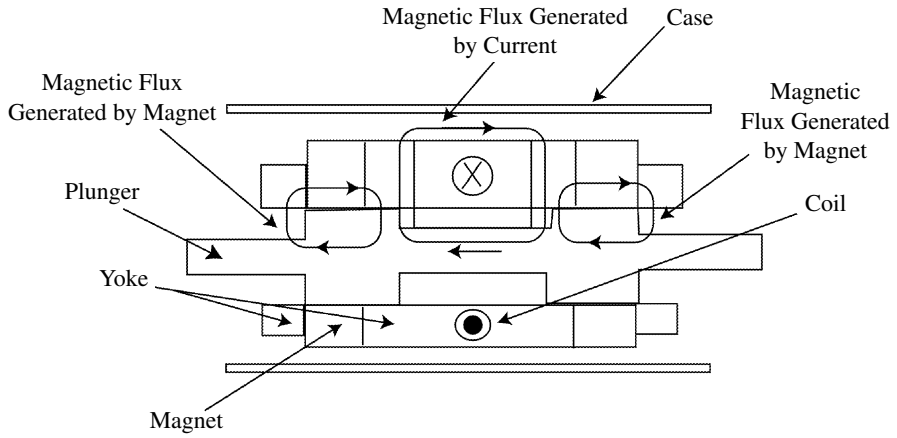

Figure 1
Magnetic drive system

sirable to stabilize its input/output relationship for each stroke. Thus, we set up five levels (k_1 to k_5) as an indicative factor (Table 5).

Considering a dynamic movement, we hoped the slope of the difference between each stroke would be flat. Yet since it can be adjusted afterward, we prioritized the system's functionality and planned to confirm the slope as a reference later.

Finally, we assigned all factors to an L_{18} orthogonal array (Table 6). Control factors are allocated to the inner array and signal, compounded noise, and indicative factors are laid out in the outer array.

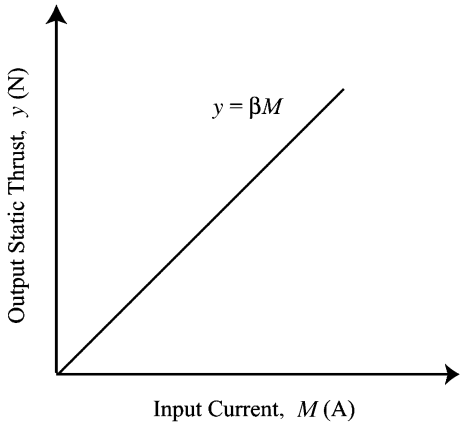

Figure 2
Ideal state

3. SN Ratio

Based on the L_{18} orthogonal array, we obtained the data shown in Table 7. Using the zero-point proportional equation, we analyzed them using the following calculation procedure.

Total variation:

$$S_T = \sum y_{ij}^2 \qquad (f = 30) \tag{1}$$

Effective divider:

$$r = \sum M_j^2 \tag{2}$$

Linear equations:

$$\begin{aligned} L_1 &= M_1 y_{11} + M_2 y_{12} + M_3 y_{13} \\ &\vdots \\ L_{10} &= M_1 y_{101} + M_2 y_{102} + M_3 y_{103} \end{aligned} \tag{3}$$

Slope:

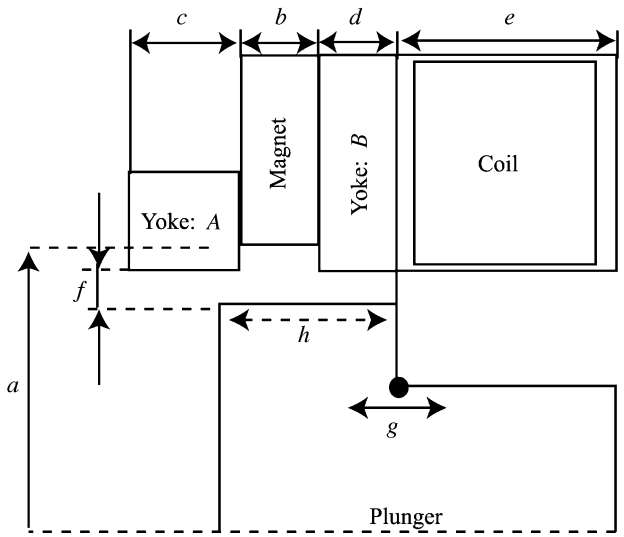

a: Internal Diameter of Magnet
b: Width of Magnet
c: Width of Yoke A
d: Width of Yoke B
e: Width of Bobbin
f: Air Gap
g: Position of Convex Portion of Plunger
h: Width of Convex Portion of Plunger

Figure 3
Magnetic drive and design parameters

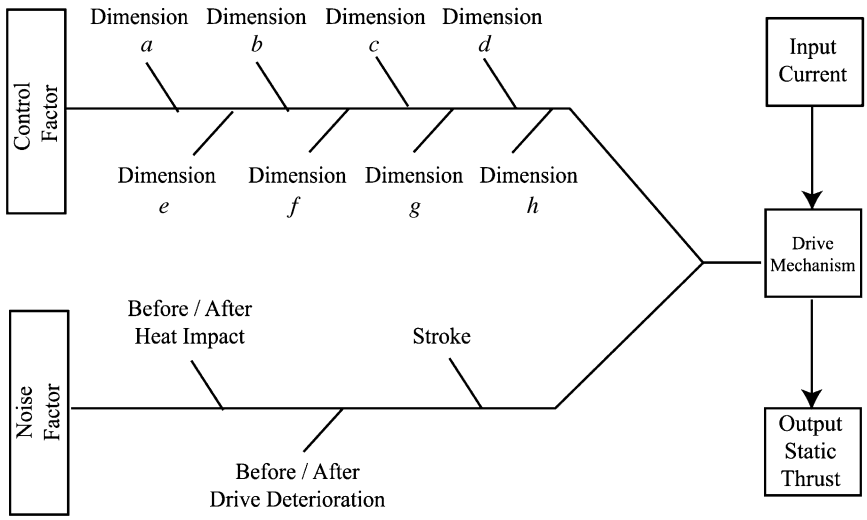

Figure 4
Y-type cause-and-effect diagram

Table 1
Control factors and levels

Control Factor		Level 1	Level 2	Level 3
A:	dimension *e*	A_1	A_2	—
B:	dimension $b + c + d$	B_1	B_2	B_3
C:	(dimension $c + d$)/factor *B*	C_1	C_2	C_3
D:	(dimension *d*)/(dimension $c + d$)	D_1	D_2	D_3
E:	dimension *a*	E_1	E_2	E_3
F:	dimension *f*	F_1	F_2	F_3
G:	dimension *g*	G_1	G_2	G_3
H:	dimension *h*/(factor *B*)	H_1	H_2	H_3

Table 2
Layout and results of L_{12} orthogonal array

	Factor								
No.	***P***	***Q***	***R***	***S***	***T***	***U***	***V***	***W***	**Data**
1	1	1	1	1	1	1	1	1	2.95
2	1	1	1	1	1	2	2	2	3.12
⋮	⋮	⋮	⋮	⋮	⋮	⋮	⋮	⋮	⋮
11	2	2	1	2	1	2	1	1	3.85
12	2	2	1	1	2	1	2	1	2.80

Table 3
Factor levels of preliminary experiment

Control Factor		Positive Side 1	Negative Side 2
P:	dimension *e*	$e + \alpha e$	$e - \alpha e$
Q:	dimension *c*	$c + \alpha c$	$c - \alpha c$
R:	dimension *d*	$d + \alpha d$	$d - \alpha d$
S:	dimension *a*	$a + \alpha a$	$a - \alpha a$
T:	dimension *b*	$b + \alpha b$	$b - \alpha b$
U:	dimension *f*	$f + \alpha f$	$f - \alpha f$
V:	dimension *g*	$g + \alpha g$	$g - \alpha g$
W:	dimension *h*	$h + \alpha h$	$h - \alpha h$

$$\beta_m = \frac{L_m + L_{m+5}}{2r} \tag{4}$$

Variation of proportional term:

$$S_\beta = \frac{\left(\sum L_i\right)^2}{10r} \qquad (f = 1) \tag{5}$$

Variation of proportional term due to stroke:

$$S_{K\beta} = \frac{1}{2r}\left[\begin{array}{l}(L_1 + L_6)^2 + (L_2 + L_7)^2 \\ + (L_3 + L_8)^2 + (L_4 + L_9)^2 \\ + (L_5 + L_{10})^2\end{array}\right] - S_\beta \qquad (f = 4) \tag{6}$$

Variation of proportional term due to compounded noise:

Table 4
Factor effects of preliminary experimental data

	Factor							
No.	*P*	*Q*	*R*	*S*	*T*	*U*	*V*	*W*
1	3.17	3.17	3.18	3.04	3.19	2.90	3.29	3.30
2	3.18	3.19	3.18	3.32	3.17	3.46	3.07	3.06

$$S_{N\beta} = \frac{1}{5r}\left[(L_1 + \cdots + L_5)^2 + (L_6 + \cdots + L_{10})^2\right] - S_\beta \qquad (f = 1) \tag{7}$$

Error variation:

$$S_e = S_T - S_\beta - S_{K\beta} - S_{N\beta} \qquad (f = 24) \tag{8}$$

Error variance:

$$V_e = \frac{S_e}{f_e} \tag{9}$$

Total error variation:

$$S_N = S_T - S_\beta - S_{K\beta} \qquad (f = 25) \tag{10}$$

Total error variance:

$$V_N = \frac{S_N}{25} \tag{11}$$

SN ratio:

$$\eta = 10 \log \frac{(1/10r)(S_\beta - V_e)}{V_N} \text{ dB} \tag{12}$$

Sensitivity:

$$S = 10 \log \frac{1}{10r}(S_\beta - V_e) \text{ dB} \tag{13}$$

SN Ratio of Slope β (Flatness)

Using β_1 to β_5, we computed nominal-the-best SN ratio as follows:

$$\eta_\beta = 10 \log \frac{\frac{1}{5}(S_m - V_N)}{V_{N'}} \text{ dB} \tag{14}$$

4. Optimal Condition and Confirmatory Experiment

SN ratios and sensitivity for each experiment are summarized in Table 8 and the factor effects are

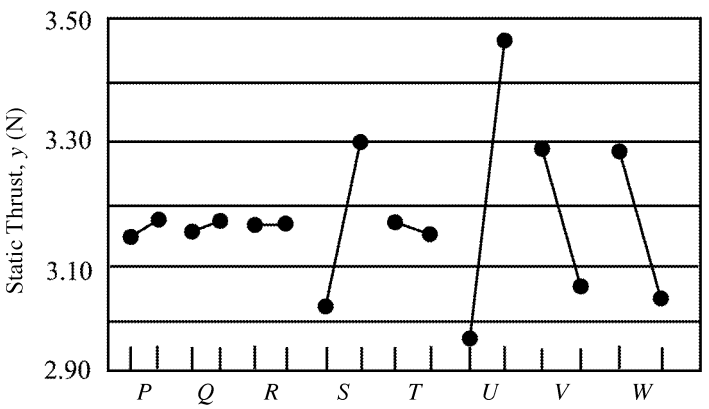

Figure 5
Response graphs for preliminary experiment

Table 5
Compounded noise factors and levels

Control Factor	Positive Side N_1	Negative Side N_2
S: dimension a	$\alpha + \alpha a$	$\alpha - \alpha a$
U: dimension f	$f + \alpha f$	$f - \alpha f$
V: dimension g	$g - \alpha g$	$g + \alpha g$
W: dimension h	$h - \alpha h$	$h + \alpha h$

illustrated in Figure 6. According to the response graphs, we determined the optimal configuration by selecting levels leading to greater SN ratios and sensitivities.

$$\textit{Optimal configuration:} \quad A_2B_3C_3D_2E_1F_2G_2H_2$$

$$\textit{Current configuration:} \quad A_1B_2C_2D_2E_2F_2G_2H_2$$

According to the magnitude of factor effects, we estimated SN ratio by factors B, C, D, F, and H and sensitivity by factors B, C, F, G, and H at the optimal and current configurations selected. Also, as shown in Table 9, we confirmed reproducibility through confirmatory experiments for the optimal and current configurations. Whereas we obtained good reproducibility of the SN ratio, we did not for sensitivity. However, we considered this not so critical because of the large gain in sensitivity.

5. Confirmation of Simulated Results Using Actual Device

Using the optimal and current configurations obtained from simulation, we prepare an actual device equipped with actual condition of use and stress (before/after thermal shock and continuous operation). As a result we obtained a large amount of gain (Table 10). Despite different absolute values of SN ratios and sensitivities, we found a correlation between the results in simulation and the actual device, which enabled us to ensure robustness in simulation. Figure 7 shows actual data at the optimal and current configurations.

On the other hand, the fact that a difference between each slope of stroke was also improved by approximately 3 dB proves that we do not have any problems in dealing with dynamic movement. Since we confirmed that simulation enables us to ensure robustness and reproducibility, by implementing product development in a small scale for the same series of products without prototyping, we can expect to reduce development labor hours and innovate our development process.

The expected benefits include elimination of the prototyping process (cut development cost in half) and a shortened development cycle time (cut labor hours for development in half). Although we focused on static simulation in this research, we will attempt to apply this technique to dynamic simulation or other mechanisms to innovate our development process and, consequently, standardize our de-

Table 6
Layout of an L_{18} orthogonal array

					N_1			N_2		
No.	1 A	2 B	⋯	8 H	M_1 k_1–k_5	M_2 k_1–k_5	M_3 k_1–k_5	M_1 k_1–k_5	M_2 k_1–k_5	M_3 k_1–k_5
1	1	1	⋯	1	⋯	⋯	⋯	⋯	⋯	⋯
2	1	1	⋯	2	⋯	⋯	⋯	⋯	⋯	⋯
⋮	⋮	⋮	⋯	⋮						
17	2	3	⋯	3	⋯	⋯	⋯	⋯	⋯	⋯
18	2	3	⋯	1	⋯	⋯	⋯	⋯	⋯	⋯

Table 7
Results of experiments

Noise	Stroke	M_1	M_2	M_3	L	β
N_1	k_1	y_{11}	y_{12}	y_{13}	L_1	β_1
	k_2	y_{21}	y_{22}	y_{23}	L_2	β_2
	k_3	y_{31}	y_{32}	y_{33}	L_3	β_3
	k_4	y_{41}	y_{42}	y_{43}	L_4	β_4
	k_5	y_{51}	y_{52}	y_{53}	L_5	β_5
N_2	k_1	y_{61}	y_{62}	y_{63}	L_6	
	k_2	y_{71}	y_{72}	y_{73}	L_7	
	k_3	y_{81}	y_{82}	y_{83}	L_8	
	k_4	y_{91}	y_{92}	y_{93}	L_9	
	k_5	y_{101}	y_{102}	y_{103}	L_{10}	

Table 8
Results of SN ratio and sensitivity analysis

No.	SN Ratio	Sensitivity	SN Ratio of Slope
1	17.97	3.55	30.10
2	25.79	8.72	18.55
3	21.42	7.49	17.15
4	18.51	8.54	14.96
5	17.28	3.15	26.28
6	28.60	9.67	24.28
7	28.09	8.71	22.38
8	23.08	9.51	25.23
9	37.14	8.15	23.12
10	23.65	5.83	25.10
11	20.33	7.71	15.33
12	29.83	7.71	24.57
13	29.41	10.20	14.10
14	29.66	7.74	26.29
15	25.02	7.26	20.82
16	21.37	4.76	22.53
17	21.10	8.56	21.36
18	30.88	9.68	17.28
Average	24.95	7.61	21.64

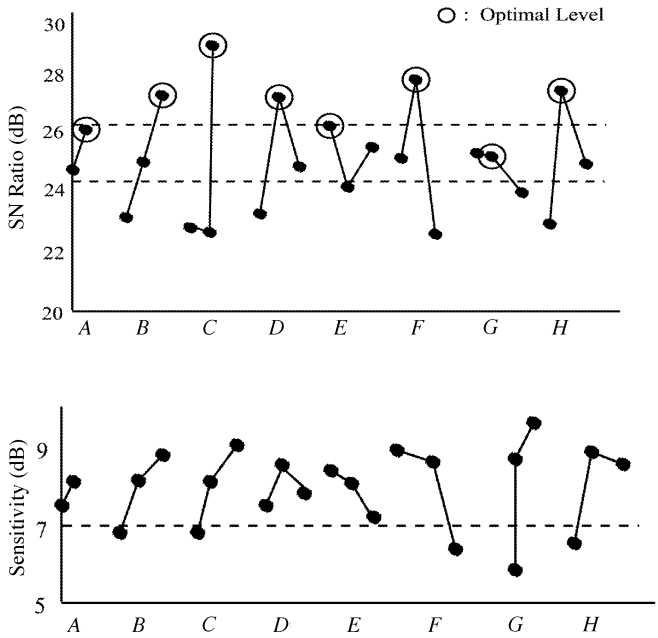

Figure 6
Response graphs

Table 9
Estimation and confirmation of gain

	Estimation		Confirmation	
Condition	**SN Ratio**	**Sensitivity**	**SN Ratio**	**Sensitivity**
Optimal	37.54	10.56	34.08	9.01
Current	29.41	9.33	27.82	9.22
Gain	8.14	1.23	6.16	−0.021

Table 10
Results confirmed by actual experimental device

Condition	SN Ratio	Sensitivity	SN Ratio of Slope
Optimal	36.43	8.97	24.22
Current	25.50	8.65	21.15
Gain	10.93	0.32	3.07

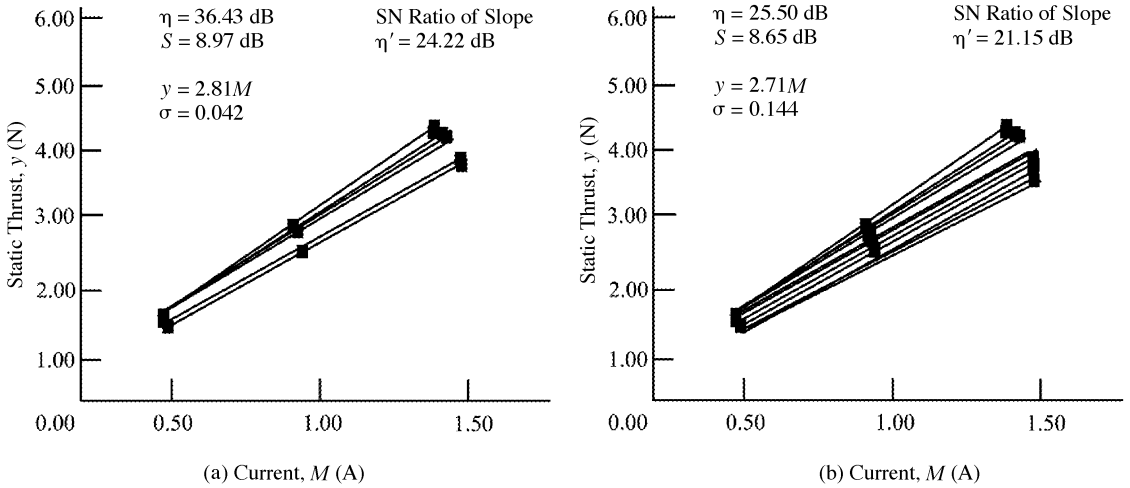

Figure 7
Confirmation of simulated results using actual device

sign process and deploy it companywide in the future.

Reference

Tetsuo Kimura, Hidekazu Yabuuchi, Hiroki Inoue, and Yoshitaka Ichii. 2001. Optimization of linear actuator using simulation. *Proceedings of the 2001 Quality Engineering Symposium*, pp. 246–249.

This case study is contributed by Tetsuo Kimura, Hidekazu Yabuuchi, Hiroki Inoue, and Yoshitaka Ichii.